Materials Reports: Energy 5 (2025) 100356

Contents lists available at ScienceDirect

Materials Reports: Energy

journal homepage: www.keaipublishing.com/en/journals/materials-reports-energy

Progress Report

Multi-scale modeling of the multi-phase flow in water electrolyzers for green hydrogen production

Lizhen Wu [a], Qing Wang [a], Wenzhi Li [a], Mingcong Tang [a], Liang An [a,b,*]

[a] Department of Mechanical Engineering, The Hong Kong Polytechnic University, Hung Hom, Kowloon, Hong Kong Special Administrative Region of China
[b] Research Centre for Carbon-Strategic Catalysis, The Hong Kong Polytechnic University, Hung Hom, Kowloon, Hong Kong Special Administrative Region of China

ARTICLE INFO

Keywords:
Water electrolyzers
Bubble dynamics
Multi-scale
Multi-phase
Modeling

ABSTRACT

Water electrolyzers play a crucial role in green hydrogen production. However, their efficiency and scalability are often compromised by bubble dynamics across various scales, from nanoscale to macroscale components. This review explores multi-scale modeling as a tool to visualize multi-phase flow and improve mass transport in water electrolyzers. At the nanoscale, molecular dynamics (MD) simulations reveal how electrode surface features and wettability influence nanobubble nucleation and stability. Moving to the mesoscale, models such as volume of fluid (VOF) and lattice Boltzmann method (LBM) shed light on bubble transport in porous transport layers (PTLs). These insights inform innovative designs, including gradient porosity and hydrophilic-hydrophobic patterning, aimed at minimizing gas saturation. At the macroscale, VOF simulations elucidate two-phase flow regimes within channels, showing how flow field geometry and wettability affect bubble discharging. Moreover, artificial intelligence (AI)-driven surrogate models expedite the optimization process, allowing for rapid exploration of structural parameters in channel-rib flow fields and porous flow field designs. By integrating these approaches, we can bridge theoretical insights with experimental validation, ultimately enhancing water electrolyzer performance, reducing costs, and advancing affordable, high-efficiency hydrogen production.

1. Introduction

The global energy use heavily relies on fossil fuels, exacerbating environmental issues such as climate change. While renewable sources like solar and wind energy offer sustainable alternatives, their potential is often limited by intermittency and geographical constraints.[1,2] In this context, hydrogen has emerged as a vital energy carrier, facilitating the storage and transportation of renewable energy without carbon emissions.[3] Among hydrogen production methods, water electrolyzers powered by renewables stand out for their environmental advantages.[4] For instance, proton exchange membrane water electrolyzer (PEMWE) faces efficiency limitations due to high cost and low hydrogen yield rate. Addressing these challenges requires not only advanced materials but also a fundamental understanding of complex multiphase phenomena, particularly bubble dynamics.[5,6]

A typical PEMWE comprises several essential components, as detailed in Fig. 1. The Hydrogen Evolution Reaction (HER) occurs at the cathode, and the Oxygen Evolution Reaction (OER) occurs at the anode. These reactions involve intricate multi-physical and chemical processes, including interactions among gas, water, heat, and electricity.[6] Bubble dynamics at the anode significantly influence overall performance. During operation, bubble evolution—encompassing nucleation, growth, and detachment—occurs at the catalyst layer (CL). The generated bubbles then enter the porous transport layer (PTL), where they are transported by capillary forces before breaking through into the anode channel, moving along the flow of water (Fig. 1). To achieve higher rates of hydrogen production, operating current densities are often raised to 10 A cm^{-2}[7] significantly boosting oxygen production within the CL. This can lead to a transition from bubble flow to plug flow and annular flow within the channel. Excessive oxygen accumulation in the channel (as seen in plug or annular flow) impedes the supply of liquid water to the electrochemical reaction sites in the CL and obstructs the expulsion of oxygen from the CL to the channel.[8] This bottleneck impacts heat and mass transfer[9] and can even lead to cell failure.[10]

* Corresponding author. Department of Mechanical Engineering, The Hong Kong Polytechnic University, Hung Hom, Kowloon, Hong Kong Special Administrative Region of China.
E-mail address: liang.an@polyu.edu.hk (L. An).
Peer review under the responsibility of Editorial Office of Chongqing Xixin Tianyuan Data & Information Co., Ltd.

https://doi.org/10.1016/j.matre.2025.100356
Received 21 April 2025; Received in revised form 21 May 2025; Accepted 29 May 2025
Available online 5 August 2025

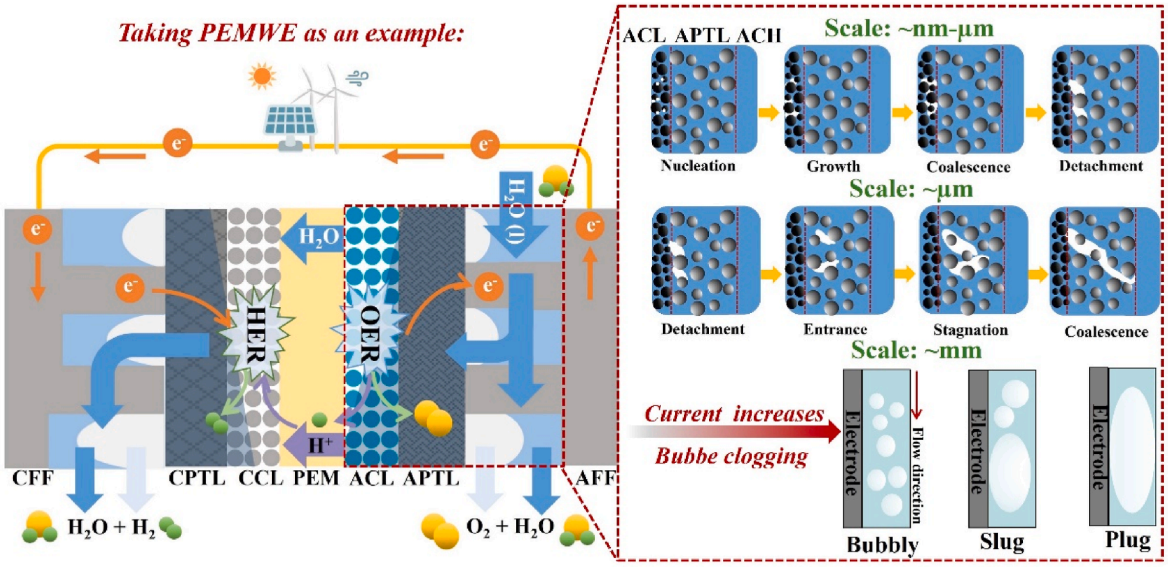

Fig. 1. Taking PEMWE as an example, bubble behaviors at different scales.

Many visualization tools like high-speed imaging[5] and X-ray tomography[11] are used to explore bubble dynamics in water electrolysis, but each has limitations. Specifically, high-speed imaging sacrifices resolution and may miss tiny bubbles. X-ray tomography can observe bubble transport in porous media, but requires costly equipment and struggles with real-time imaging of fast processes and high gas content.[12] To address these issues, recent advancements in multi-scale and multi-phase modeling, alongside innovative visualization techniques, have begun to elucidate the complex relationship between bubble behavior and electrochemical performance. At the nanoscale, molecular dynamics (MD) investigates[13–15] the impact of various surface structures on the nucleation and growth of nanobubbles in nanoelectrodes. At the microscale, pore-level models including the volume of fluid (VOF) method,[16–18] lattice Boltzmann method (LBM),[19–21] pore network model (PNM),[22,23] and phase field methods (PFM)[24–26] can simulate bubble transport within the PTL, revealing how surface wettability and PTL morphology influence gas saturation. The VOF method also clarifies bubble transport from the PTL to the channel, which informs flow field designs.[27] Traditional physical models, like VOF, often encounter computational inefficiencies, prompting the integration of artificial intelligence (AI) techniques to enhance analyses. Machine Learning (ML), as an AI framework, autonomously learns from data,[28] optimizing various factors and improving the performance of water electrolyzers and bubble distribution.[5] This synergy substantially reduces computational complexity and accelerates research cycles. Furthermore, it is important to note that these models can complement advanced visualization tools, such as high-speed imaging, X-ray tomography, and synchrotron radiation imaging.

This review focuses on advances in multi-scale and multi-phase modeling as complementary visualization techniques for analyzing bubble dynamics in water electrolyzers. First, we analyze the application of different models for bubble visualization at different scales, such as MD for nanobubbles in CL, VOF and LBM for microbubbles in PTL, and VOF for macrobubbles in the channel. At the same time, we critically assess the strengths and weaknesses of the different models and highlight their advantages in predicting gas-liquid interactions and guiding material/structural innovations. We then discuss how cutting-edge AI-driven models can accelerate the computations of the aforementioned physical models and related optimization. Finally, we point out persistent challenges, including the need for unified models that combine bubble dynamics with electrochemical degradation mechanisms, and suggest future research directions to accelerate the commercialization of water electrolyzers such as PEMWE. By synthesizing these insights, this study aims to lay the groundwork for a next-generation water electrolyzer design that prioritizes efficient bubble management, ultimately enabling affordable large-scale green hydrogen production.

2. Molecular dynamics simulation for nanobubbles in the electrode

MD simulation serves as an effective tool for observing electrochemically generated nanobubbles on nanoelectrodes by calculating the forces acting on each molecule or atom within a specified volume, thereby determining their trajectories over time.[29] It provides higher spatial and temporal resolution, complementing the findings of experimental studies and providing additional insights into the molecular pathways involved in the nucleation process of nanobubbles.[30] To accurately capture bubble behaviors at such small scales, MD simulations require time steps that align with molecular motion, typically on the order of femtoseconds (fs). Furthermore, given the number of atoms and degrees of freedom, MD simulations are restricted to nanoscopic regions and process time scales of 100 ns.[31] The choice of force field in MD simulations is critical and significantly impacts the accuracy of the results. For example, ReaxFF[32] is employed to simulate the generation of nanobubbles from nanoelectrodes in water electrolysis. Non-reactive force fields, such as the Lennard-Jones,[33,34] can also be utilized to simulate interactions between molecules. However, to reduce calculation costs, a monatomic coarse-grained method is generally adopted to model all molecules. In this model, water interactions are represented by the monatomic water (MW) potential that simplifies the representation to a single site, while the Stillinger-Weber (SW) potential is employed to account for interactions among water molecules. This includes both two-body and three-body potentials. The surface tension is set at $\gamma = 0.072$ N m^{-1}. Within this framework, the three-body potential effectively simulates the intricacies of water interactions, while two-body potentials are used to model interactions between different atoms. The specific expressions for these potentials are available in Refs. 13,35.

$$U_{(r)} = \sum_i \sum_{j>i} \phi_2(r_{ij}) + \sum_i \sum_{j\neq i} \sum_{k>j} \phi_3(r_{ij}, r_{ik}, \theta_{ijk}) \tag{1}$$

$$\phi_2(r) = A\varepsilon\left[B\left(\frac{\delta}{r}\right)^p - \left(\frac{\delta}{r}\right)^q\right]\exp\left(\frac{\delta}{r - a\delta}\right) \tag{2}$$

$$\phi_3(r,s,\theta) = \lambda\varepsilon[\cos\theta - \cos\theta_0]^2 \exp\left(\frac{\gamma^\delta}{r-a\delta}\right)\exp\left(\frac{\gamma^\delta}{s-a\delta}\right) \quad (3)$$

Where ϕ_2 and ϕ_3 are the two-body potential and three-body potential, respectively. λ and θ determine the interaction strength and angle between the three-body potential ($\lambda = 23.15$, $\theta = 109.47°$). ε and δ determine the interaction strength and scale between pair potential. The inter-particle distance r and a cut-off radius of $a = 1.8$ ensure all potentials and forces in the SW model are zero for $r \geq a\ \delta$. A harmonic potential with a constant of 10 kcal mol^{-1} Å^{-2} simulates vibrations of solid and electrode molecules, preserving their overall structure.

At the very beginning, Weijs et al.[36] used molecular dynamics simulations to investigate the behavior of surface nanobubbles in a ternary system (gas, liquid, solid) comprising Lennard-Jones fluids. Their findings revealed that these nanobubbles formed under conditions of sufficiently low gas solubility in the liquid, effectively meaning a high relative gas concentration. When the gas-solid interaction was notably strong, the surface nanobubbles resided on a gas layer that developed between the liquid and the solid, which played a crucial role in determining the contact angle derived from microscopic parameters. However, the drawback is that the gas bubbles are not considered electrochemically generated. Subsequently, Perez Sirkin et al.[37] were the first to investigate the molecular dynamics of electrochemically generated nanobubbles. They simulated a system consisting of a $10 \times 10 \times 15$ nm^3 box containing 33,400 water molecules over a 100 ns duration, aiming to understand the nucleation and stationary state of individual nanobubbles formed on a nanoelectrode (Fig. 2a). One of the important findings is that once the critical size of gas molecule clusters exceeds ~0.5 nm (equivalent to about 30 gas molecules), the formation of stable nanobubbles on the nanoelectrode occurs within roughly 20 ns. The critical bubble cluster diameter closely matches the experimentally estimated number of gas molecules in the bubble core. Furthermore, the potential dependence and molecular dynamics of electrochemical reactions were simulated and verified using an analytical model combined with kinetic Monte Carlo simulations by Gadea et al. (Fig. 2b).[35–38] They found that the use of small arrays of nano-electrodes, rather than larger individual electrodes, offers significant advantages in maximizing the current and conversion rate of the gaseous generation reaction due to

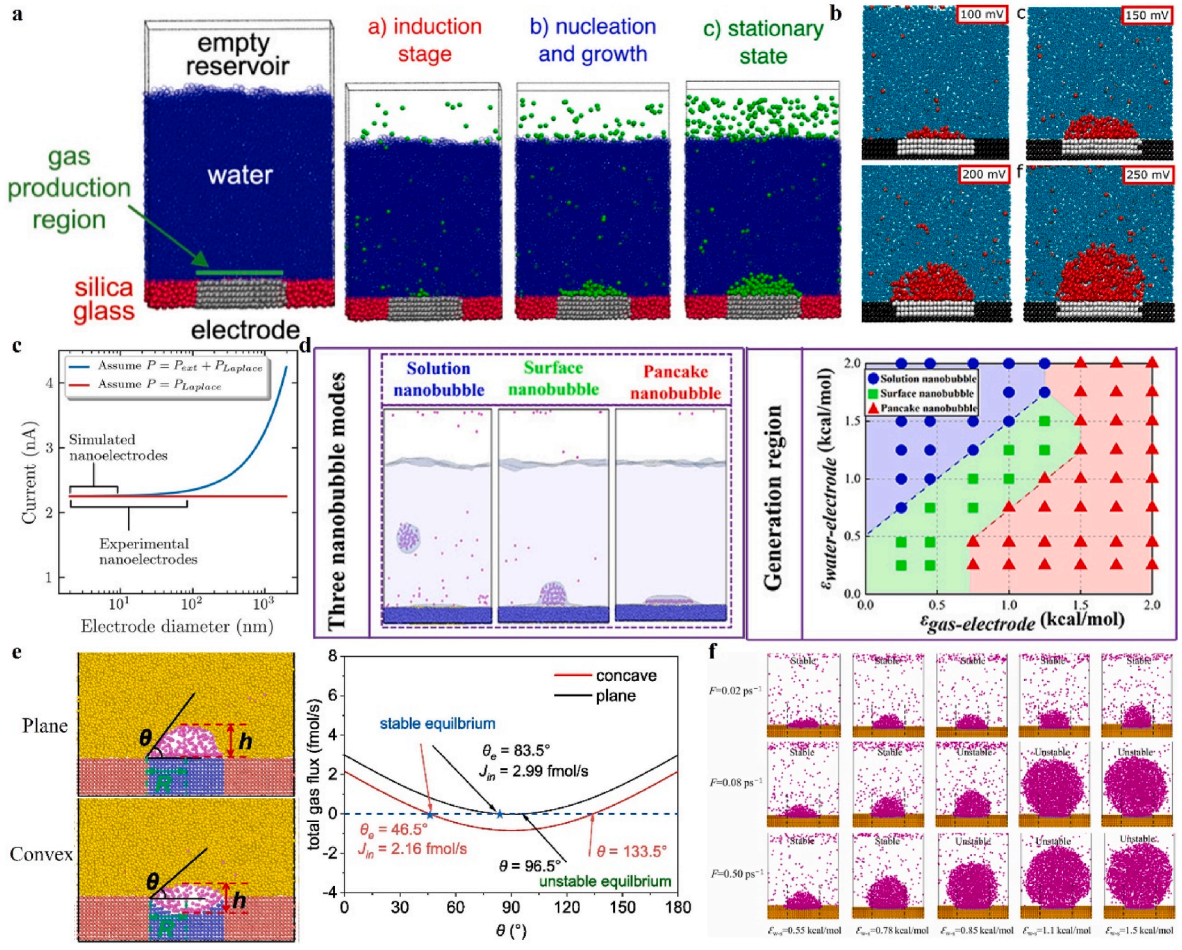

Fig. 2. (a) Schematic representation of the simulation cell depicting the formation of a surface nanobubble. Particles of the silica-like amorphous solid wall, electrode, liquid water, and gas are illustrated in red, gray, blue, and green, respectively. Stages of bubble formation include induction, nucleation, and growth (where the cluster exceeds critical size and shows a low contact angle of ~20°), and the stationary state. Reproduced with permission from Ref. 37. (b) Representative cross-sectional snapshots of stationary bubbles in simulations, illustrating size and geometry variations for potential ΔE between 100 and 250 mV at a 5 nm diameter electrode. Water molecules are shown in blue, gas molecules in red, electrode particles in white, and inert wall particles in black. (c) Residual currents as a function of electrode diameter. Reproduced with permission from Ref. 38. (d) Snapshots from MD simulations of nucleated nanobubbles and phase maps of three modes based on relative surface energies: (left) electrolyte-electrode energy > gas-electrode energy, (middle) electrolyte-electrode energy ≈ gas-electrode energy, and (right) electrolyte-electrode energy < gas-electrode energy. Reproduced with permission from Ref. 39. (e) Schematic representation of nanobubble geometric parameters on various nanostructured surfaces, illustrating the relationship between contact angle and total gas flux. Reproduced with permission from Ref. 13. (f) MD snapshots of stable (65 ns) and unstable nanobubbles (pre-detachment) for various $\varepsilon_{w\text{-}s}$ and conversion rates F. Dashed lines denote the edges of the left and right electrodes. Reproduced with permission from Ref. 35.

the compensating effects of bubble area growth and Laplace pressure (Fig. 2c). To further elucidate the dynamics at the electrode interface and to ensure correlation with real-world hydrogen evolution scenarios, Li et al.[39] developed a self-programming gas generation algorithm to simulate continuous gas generation. This algorithm operates on the principle of hydrogen generation at the electrode surface during water electrolysis, introducing gas molecules at intervals of $1/f$ ps intervals, where $f = 0.02$ ps^{-1} from experimental data, thus linking the simulation to actual observations. As the gas accumulates, it inhibits the electrochemical reaction by decreasing the accessibility of water to the reaction site. The algorithm ensures that the gas is formed only when water is present. Given the stochastic nature of molecular distribution, the simulation allows up to 10 attempts to correctly position the generated gas molecules. If unsuccessful, the simulation proceeds after a delay of $1/f$ ps. They identified three different types of nanobubbles: surface nanobubbles, solution nanobubbles, and pancake nanobubbles, each exhibiting unique interfacial behaviors based on electrode properties. Solution nanobubbles formed mainly on hydrophilic electrodes, pancake nanobubbles were attached to hydrophobic electrodes, and surface nanobubbles were in the form of spherical caps (Fig. 2d).

The maturation of this model lays the groundwork for exploring how the surface morphology[13–15] and surface wettability[35] of electrodes influence nanobubble behaviors, facilitating more informed electrode designs. Regarding surface morphology, Nie et al.[13] demonstrated that during the stabilization stage, nanobubbles on a planar surface exhibit a contact angle of 34.6° and a contact radius 3 Å larger than those on a concave surface, with heights remaining consistent at about 20 Å. The reaction rate on the planar surface is higher, indicating that water molecules are more accessible to gas molecules there. A dynamic equilibrium model reveals that gas flux on the concave surface is lower, resulting in a smaller contact angle, which suggests that the concave geometry restricts the movement of water and gas to the electrode (Fig. 2e). In terms of wettability, Zhan et al.[35] discovered that the morphology, size, and stability of nanobubbles closely correspond to the conversion rate F and the surface wettability ($\varepsilon_{w\text{-}s}$) of the surrounding solid plate. When $\varepsilon_{w\text{-}s}$ is lower than a certain critical value, stable nanobubbles can be formed regardless of the value of F. On the contrary, stable nanobubbles are more likely to form at low values of F when $\varepsilon_{w\text{-}s}$ is high. However, when F experienced a slight increase while $\varepsilon_{w\text{-}s}$ remains high, the grown nanobubbles are more likely to become unstable and detach from the electrode surface (Fig. 2f).

3. Mesoscale simulation for bubble transport in porous transport layer

The bubbles originate from the electrode and migrate into the PTL, subsequently being transported into the channel via capillary forces, with their behaviors constrained to the micron scale. A variety of mesoscopic models have been developed to simulate bubble behavior in PTLs that closely resemble realistic scenarios. For example, Notable methods for capturing and tracking interfaces between gas and liquid include the volume of fluid method (VOF),[16–18] the lattice Boltzmann method (LBM),[19–21] the pore network method (PNM),[22,23] and the phase field method (PFM)[24–26] which are widely used to study the two-phase flow in the PTLs of water electrolyzers and have shown good numerical stability and reliability. The VOF model excels in capturing phase interfaces through a capillary pressure term in the momentum equation, but necessitates a fine mesh for accuracy.[40] LBM is effective for complex microscale geometries, naturally modeling dynamic interfaces and benefiting from GPU acceleration, although it struggles with stability at high density/viscosity ratios and demands significant memory.[41] Conversely, the PNM offers high computational efficiency for large-scale simulations and accurately predicts macroscopic properties like permeability; however, it simplifies pore structures, which may compromise accuracy regarding microscopic dynamics.[22] The PFM models diffuse interfaces and integrate well with multi-physics applications, but face challenges with high computational costs and assumptions about artificial interface thickness.[24] Consequently, selecting the appropriate model for a given situation is crucial. A summary of the advantages and disadvantages of each model is presented in Table 1.

The structural parameters (porosity, pore size/distribution) and physical properties (e.g., surface wettability) of PTL critically influence the bubble transport dynamics.[42] The models discussed not only elucidate the bubble transport mechanism in PTL but also propose innovative PTL designs through exploring the effects of the above parameters. Li et al.[43] first identified and proposed the concept of an 'isolation belt' through VOF simulation results, which is formed by a series of random narrow throats in the PTL. Its narrow throats create a large capillary resistance barrier that makes it difficult for oxygen bubbles to pass through. If the bubbles on either side of the 'barrier' cannot be met, they will not merge, resulting in a higher number of transport paths and increased oxygen saturation. Additionally, perforation may disrupt the 'isolation belt', thereby creating preferential transport pathways that help reduce oxygen saturation (Fig. 3a). Using PFM, Wu et al.[44] also demonstrated that the oblique perforation technique in the PTL significantly enhances oxygen and substantially mitigates oxygen accumulation beneath the channel ribs (Fig. 3b). Moreover, when maintaining a constant porosity in the PTL, reducing fiber diameter in the vicinity of the CL can significantly decrease the local oxygen saturation. Similar findings have been corroborated by both LBM[41,45] and PNM[22] models, which indicate that increasing porosity from the PTL-electrode interface to the PTL-flow field interface results in lower gas saturation and higher liquid water permeability. In terms of surface wettability, Li et al.[19] concluded that, although wettability impacts oxygen distribution after breakthrough, it does not alter the capillary fingering transport pattern. Weakly hydrophilic areas tend to oxygen accumulation, whereas strongly hydrophilic regions enhance oxygen processing. Yang et al.[46] proposed a design for combining strong and weak hydrophilicity at the catalyst layer end of the transport layer, which can lower oxygen saturation by up to 30% on the surface (Fig. 3c).

In terms of operating conditions, Qiu et al.[17] found that increased back pressure reduces bubble formation frequency and expulsion efficiency in the flow channel but does not alter the bubble formation process. Higher operating pressure improves gas-liquid interaction, leading to smaller bubbles. As pressure rises, the frequency of bubble generation in the flow channel increases while the bubble size decreases. At low pressure, bubbles form randomly, requiring higher water flow rates for effective management. However, because the formation mechanism stays the same, bubbles linger longer in the porous medium, resulting in lower bubble discharging efficiency. Future PTL designs can be refined to improve bubble discharging in high-pressure electrolyzers (Fig. 3d).

4. Macroscale simulation for two-phase flow in channel

The two-phase flow regimes in the channel have a significant effect

Table 1
Comparison of VOF, LBM, PNM, and PFM.

Type	Advantages	Disadvantages
VOF[40]	1. Sharp interface tracking 2. High accuracy	1. High computational cost 2. Mesh dependency
LBM[41]	1. GPU-friendly and parallel 2. Handles complex geometry 3. Mesoscopic approach 4. No explicit tracking	1. Unstable at high density/viscosity ratios 2. High memory consumption 3. Time-step limit
PNM[22]	1. Fast for large scales 2. Macroscopic predictions	1. Idealized pore networks 2. No interface dynamics
PFM[24]	1. Diffuse interfaces 2. Multi-physics coupling	1. Artificial interface thickness 2. High computational cost

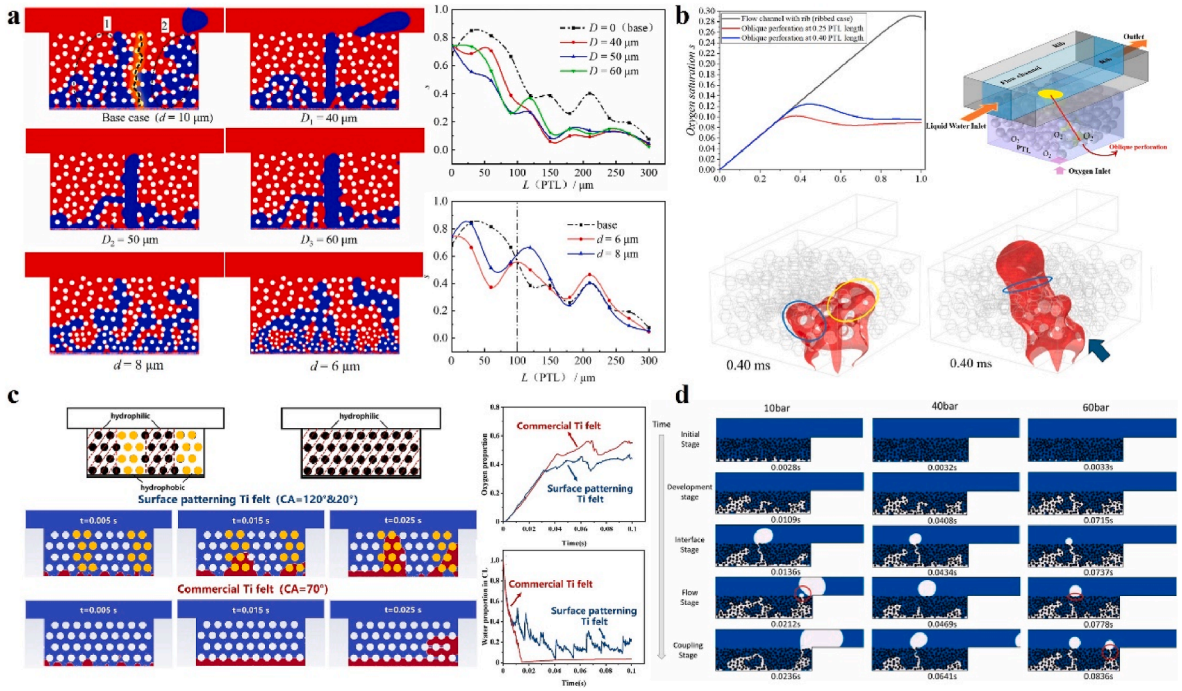

Fig. 3. (a) Effect of perforation diameters and fiber diameters on oxygen distribution. (black dashed line is isolation belt). Reproduced with permission from Ref. 43. (b) Schematic diagram of PTL oblique perforation and its oxygen breakthrough characteristics compared with the base case. Reproduced with permission from Ref. 44. (c) Hydrophilic-hydrophobic and single wettability structures and bubble transport processes within them. Reproduced with permission from Ref. 46. (d) Breakthrough process of bubbles at different pressures. Reproduced with permission from Ref. 17.

on the performance of the water electrolyzers. The two-phase flow regimes are mainly determined by the water flow rate, the oxygen generation rate and the flow field pattern.[47] A higher water flow rate[48] (Fig. 4a) and a suitable flow field, such as a parallel flow field[48] (Fig. 4b), are more favorable for the bubbles discharging. VOF is commonly employed to simulate a near-realistic two-phase flow regime within flow-field channels, thus helping to quickly screen suitable flow field designs for water electrolyzers. Initial simulations of two-phase flow in these channels were conducted by applying a constant gas velocity uniformly across the bottom surface, as demonstrated by Lafmejani et al.[49] This model was utilized to represent bubble production and simulate Taylor flow within the flow channel. Dang et al.[50] compared the results of two-phase flow simulated by VOF with experimental optical visualization results, finding excellent agreement, particularly in the transition of bubbles between bubbly flow, slug flow, and annular flow. Their results further demonstrated that the hydrophilic flow channel wall accelerates bubble discharging. Subsequently, Wu et al.[27] were pioneers in coupling the VOF model with a full-cell model to better reflect the relationship between realistic two-phase flow and the electrochemical performance of channels in PEMWE. Their model underwent rigorous validation that included examining polarization curves, ohmic losses, and the two-phase flow regimes within the parallel and serpentine flow fields (Fig. 4b). This model was mainly carried out in the following steps (Fig. 4c): A 3D full-cell simulation is first performed under the assumption that there is no oxygen in the anode channel. The oxygen flux entering the channel is then extracted and applied as a boundary condition at the channel's bottom in the VOF model. Once the average oxygen volume fraction in the channel and at the PTL surface stabilizes, this oxygen saturation distribution is used as the boundary condition for the oxygen pressure equation in the porous electrodes of the PEMEC. Although the channel's two-phase flow is unsteady, it is assumed that when the average oxygen saturation at the PTL surface is steady, the corresponding simulated distribution can be treated as a quasi-steady state. In addition, they also utilized this method to demonstrate that the structured mesh channel can split large bubbles into small bubbles compared with a single straight channel (Fig. 4d), which significantly improves the non-uniform temperature distribution and current density distribution in the electrode of PEMWE (Fig. 4e).[51] For the structured mesh channel, a design that gradually reduces the hydrophobicity (i.e., contact angle) of the skeletal surface from the top of the channel to the PTL surface contributes to the performance of the PEMWE by improving the oxygen discharging capacity. Following the work of Wu et al.,[27,51] Zhou et al.[52] developed a similar coupling method. They first used the model to explore the effect of anode PTL on two-phase flow in the flow channel. The results showed that the bubble coverage on the upper surface of the PTL decreased by 42.9% when the contact angle was reduced from 90° to 50°, which also proved its high sensitivity and could provide a valuable guide for the design of PTLs for PEMWE. Later, they expanded it from a single flow channel to a flow field scale and found that the accumulation of bubbles in the outlet manifold also affects the bubble removal rate and leads to bubble backflow. The hydrophilic anode PTL leads to a higher proportion of slug flow in the middle channel of the parallel flow field (channels 2 and 3), which reduces the bubble removal rate. To improve bubble removal efficiency, hydrophilicity must be minimized. Hydrophobic anode PTL conditions create films and wavy flow, resulting in delayed migration of bubbles towards the outlet manifold (Fig. 4f).[53]

5. AI-driven models accelerating physical models

Traditional physical models like the VOF method exhibit computational inefficiencies, prompting the integration of AI techniques to enhance theoretical analyses.[54] ML, an AI framework grounded in statistical methods, can autonomously learn from prior data,[55] enabling optimization across a spectrum of variables—from atomic-level descriptors to macro-engineering factors—ultimately improving water electrolyzer performance and bubble distribution. The most significant benefit of this synergy is the ability to eliminate complex computational processes,[56] thereby shortening research cycles.[57] AI-based data-driven models, such as artificial neural networks (ANN)[58] and support vector

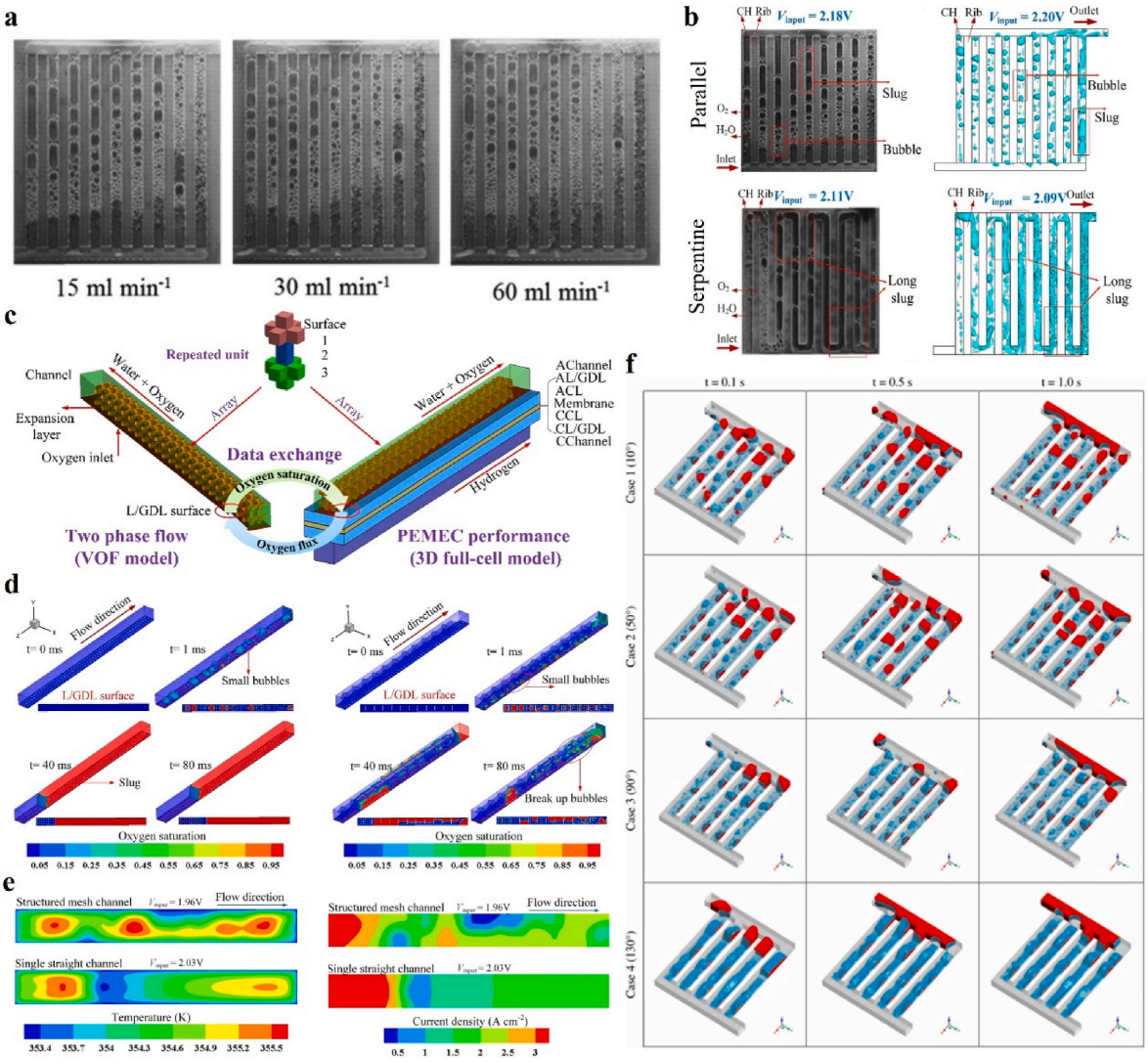

Fig. 4. (a) Effect of water flow rate on two-phase flow in flow field. Reproduced with permission from Ref. 48. (b) Comparison between simulation results and the experimental results. Reproduced with permission from Ref. 51. (c) Schematic of data exchange between VOF and 3D full-cell models. (d) Simulated two-phase flow in straight channel and structured mesh channel. (e) Temperature and current density distributions in CL. Reproduced with permission from Ref. 51. (f) Changes in two-phase flow regimes with constant contact angles of anode PTL. Reproduced with permission from Ref. 53.

machines (SVM),[59] provide alternative tools for R&D in everything from lithium batteries to PEM fuel cells. A comprehensive review of AI-based approaches to the digitization of porous energetic materials is provided by Niu et al.[28] For water electrolyzer, Chen et al. combined a multi-physics coupled model with a data-driven alternative model (i.e., ANN) to obtain an optimal channel width and an optimal depth of 2 mm, resulting in 38.61% of the current density.[60] In addition, certain AI algorithms, such as genetic algorithms (GA), can be used to efficiently optimize to obtain the best value. For example, Wang et al.[59] used a genetic algorithm to identify the optimal MEA for a PEM fuel cell. However, AI-assisted optimization of the bubble visualization physics model for water electrolyzers is scarce, and we aim to provide some prospective cases to provide theoretical guidance.

An example of AI-accelerated physical modeling is the work by Wu et al.,[5] who designed a dual-layer channel (the degassing layer is tightly installed on the base layer) that enhances the self-pumping effect by leveraging capillary pressure differences, reducing bubble coverage on the electrode surface (Fig. 5a and b). This design achieved improved cell performance (~0.15 V at 5.0 A cm^{-2}) compared to traditional single-layer systems. To explore bubble behaviors, the VOF model assessed the impact of various degassing layers and base layer heights, but the multitude of potential configurations made this approach computationally demanding. To address this challenge, a data-driven surrogate model based on a deep neural network (DNN) was developed and trained using data from the VOF method (Fig. 5c).[61] Utilizing this efficient surrogate model, the optimal dimensions of the base and degassing layers were identified through a GA. The efficacy of this optimization was validated through experimental bubble visualization and electrochemical characterization in PEMWE. The geometry of flow fields with channels and ribs is relatively easy to design and fabricate, with many studies focusing on structural optimization. However, optimizing porous flow fields is still in its early stages. Although 3D printing effectively creates porous structures, the technique can be expensive and may distort materials during production. Additionally, reconstructing porous structures and generating meshes for numerical calculations is more complex and time-consuming than for channel-rib configurations. However, using porous structures allows for greater flexibility in design and optimization in 3D space, as factors like pore distribution, skeleton structure, and wettability can be adjusted more easily. Zhang et al.[62] first reconstructed the porous media channel by simplifying it into a structured mesh channel (Fig. 5d). They then obtained a large amount of training data from a validated 3D multiphase non-isothermal model and

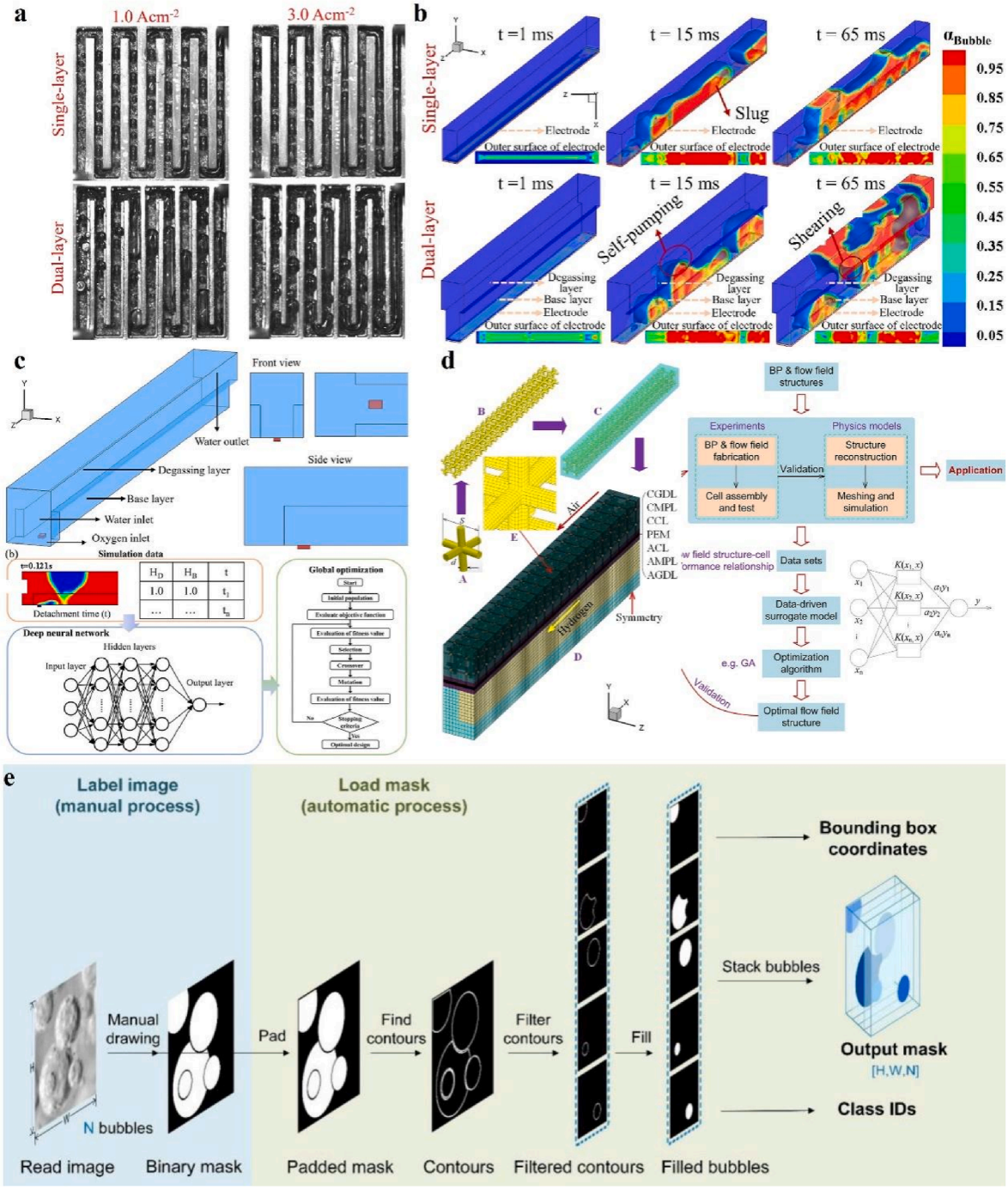

Fig. 5. (a) Visualization of two-phase flow regimes in single-layer flow field and dual-layer flow field. (b) Simulation of bubble behaviors in single-layer and dual-layer designs. Reproduced with permission from Ref. 5. (c) Computational domain in physical model and optimization framework for optimization of dual-layer channel. Reproduced with permission from Ref. 61. (d) Computational domain of porous flow field and AI-assisted forward design flowchart for optimization of porous channel. Reproduced with permission from Ref. 53. (e) Manual image segmentation using OpenCV and the method for loading corresponding masks. Reproduced with permission from Ref. 64.

developed a data-driven model based on SVM to optimize the flow field geometry. They also employed a GA to enhance optimization, using the SVM model as the fitness evaluation function. The optimal values from this approach were confirmed with the 3D model, demonstrating the effectiveness of the data-driven model in designing and optimizing porous media flow fields. This method can also enhance the structured mesh channel design by Wu et al.[51]

In addition to facilitating hybrid physical-data modeling to lower measurement and computational expenses, AI also offers significant advancements in experimental studies.[63] For example, a method based on Mask R-CNN[64] can effectively assist in bubble detection, segmentation, and shape reconstruction, enabling precise quantitative analysis of bubble flows characterized by high gas holdup and substantial bubble overlap (Fig. 5e). As a powerful image analysis tool, AI enhances the accuracy and efficiency of such experimental investigations.

6. Conclusion and outlook

This review highlights significant advancements in optimizing bubble dynamics in water electrolyzers through multi-scale and multi-phase modeling. At the nanoscale, MD simulations show that surface nanostructuring and wettability influence nanobubble nucleation, with hydrophobic surfaces favoring stable bubble detachment and hydrophilic areas improving reaction access. These findings inform electrode designs, such as nanoarrays, to reduce gas blockage. Mesoscale models, including VOF, LBM, PNM, and PFM, indicate that PTLs with gradient porosity or hybrid wettability can decrease oxygen saturation by up to 30%, lowering mass transport overpotentials. Structured PTLs with customized pore distributions enhance bubble expulsion by disrupting gas isolation belts. At the macroscale, VOF models demonstrate that hydrophilic flow fields reduce bubble coalescence and backflow, while structured mesh channels promote bubble fragmentation. Additionally, AI tools like DNN and GA facilitate the optimization of channel geometries and operational parameters, reducing computational costs without sacrificing accuracy.

However, challenges persist. Current models often oversimplify the interaction between bubble dynamics and electrochemical degradation, especially under transient renewable power conditions. Moreover, experimental validation of these multi-scale simulations frequently occurs under ideal conditions, overlooking real-world complexities such as material heterogeneities and catalyst degradation. Future research should focus on integrating bubble dynamics with thermal, mechanical, and electrochemical models to better predict the relationship between bubble dynamics and device lifetimes and failure modes.

CRediT authorship contribution statement

Lizhen Wu: Writing – review & editing, Conceptualization, Writing – original draft. **Qing Wang:** Investigation. **Wenzhi Li:** Investigation. **Mingcong Tang:** Writing – review & editing. **Liang An:** Resources, Supervision, Writing – review & editing, Conceptualization.

Declaration of competing interest

The authors declare that they have no known competing financial interests or personal relationships that could have appeared to influence the work reported in this paper.

Acknowledgement

This work was supported by a grant from the Research Grants Council of the Hong Kong Special Administrative Region, China (Project No. 15308024) and a grant from Research Centre for Carbon-Strategic Catalysis, The Hong Kong Polytechnic University (CE2X).

References

1. Saeidi S, Sápi A, Khoja AH, et al. Evolution paths from gray to turquoise hydrogen via catalytic steam methane reforming: current challenges and future developments. *Renew Sustain Energy Rev*. 2023;183:113392. https://doi.org/10.1016/j.rser.2023.113392.
2. Gao X, Chen Y, Wang Y, et al. Next-generation green hydrogen: progress and perspective from electricity, catalyst to electrolyte in electrocatalytic water splitting. *Nano-Micro Lett*. 2024;16:237. https://doi.org/10.1007/s40820-024-01424-2.
3. Zang G, Graham EJ, Mallapragada D. H2 production through natural gas reforming and carbon capture: a techno-economic and life cycle analysis comparison. *Int J Hydrogen Energy*. 2024;49:1288–1303. https://doi.org/10.1016/j.ijhydene.2023.09.230.
4. Bamba JN, Dumlao AT, Lazaro RM, Matienzo DD, Ocon J. Green hydrogen from seawater electrolysis: recent developments and future perspectives. *Curr Opin Electrochem*. 2024;48:101592. https://doi.org/10.1016/j.coelec.2024.101592.
5. Wu L, Pan Z, Yuan S, et al. A dual-layer flow field design capable of enhancing bubble self-pumping and its application in water electrolyzer. *Chem Eng J*. 2024;488:151000. https://doi.org/10.1016/j.cej.2024.151000.
6. Yuan S, Zhao C, Cai X, et al. Bubble evolution and transport in PEM water electrolysis: mechanism, impact, and management. *Prog Energy Combust Sci*. 2023;96:101075. https://doi.org/10.1016/j.pecs.2023.101075.
7. Villagra A, Millet P. An analysis of PEM water electrolysis cells operating at elevated current densities. *Int J Hydrogen Energy*. 2019;44:9708–9717. https://doi.org/10.1016/j.ijhydene.2018.11.179.
8. Zhang T. Relationship of local current and two-phase flow in proton exchange membrane electrolyzer cells. *J Power Sources*. 2022;10.
9. Lasek L, Krzywanski J, Skrobek D, Zylka A, Nowak W. Review of Micro- and nanobubble technologies: advancements in theory and applications and perspectives on adsorption cooling and desalination systems. *Energies*. 2023;16:8078. https://doi.org/10.3390/en16248078.
10. Garcia-Navarro JC, Schulze M, Friedrich KA. Detecting and modeling oxygen bubble evolution and detachment in proton exchange membrane water electrolyzers. *Int J Hydrogen Energy*. 2019;44:27190–27203. https://doi.org/10.1016/j.ijhydene.2019.08.253.
11. Leonard E, Shum AD, Normile S, et al. Operando X-ray tomography and sub-second radiography for characterizing transport in polymer electrolyte membrane electrolyzer. *Electrochim Acta*. 2018;276:424–433. https://doi.org/10.1016/j.electacta.2018.04.144.
12. Maier M, Smith K, Dodwell J, Hinds G, Shearing PR, Brett DJL. Mass transport in PEM water electrolysers: a review. *Int J Hydrogen Energy*. 2022;47:30–56. https://doi.org/10.1016/j.ijhydene.2021.10.013.
13. Nie T, Xu Q, She Y, et al. The behavior of surface nanobubbles on different substrates in electrochemistry. *J Mol Liq*. 2024;394:123791. https://doi.org/10.1016/j.molliq.2023.123791.
14. Maheshwari S, van Kruijsdijk C, Sanyal S, Harvey AD. Nucleation and growth of a nanobubble on rough surfaces. *Langmuir*. 2020;36:4108–4115. https://doi.org/10.1021/acs.langmuir.0c00635.
15. Guo Z, Feng Y, Zhang H, Wang Q, Zhang X, Wang L. The behaviors of interfacial nanobubbles on flat or rough electrode surfaces in electrochemistry. *Langmuir*. 2024;40:26661–26671. https://doi.org/10.1021/acs.langmuir.4c03771.
16. Sourya DP. *A Comparative Study on the Lattice Boltzmann Method and the VoF-Continuum Method for Oxygen Transport in the Anodic Porous Transport Layer of an Electrolyzer*. vol 92. 2024:1091–1098, 1091-1098.
17. Qiu Y, Zhang R, Liu C, Liu R, Shahgaldi S, Sui P-C. Numerical investigation on two-phase flow of PEM water electrolyzers under high operating pressures. *Int J Hydrogen Energy*. 2025;105:817–834. https://doi.org/10.1016/j.ijhydene.2025.01.331.
18. Liu J, Yang Y, Kerner F, Schröder D. Unraveling the impact of compression on the performance of porous transport layers in water electrolyzers. *Appl Energy*. 2025;381:124982. https://doi.org/10.1016/j.apenergy.2024.124982.
19. Li Q, He Y, Zhang L, et al. Effect of porous transport layer wettability on oxygen transportation in proton exchange membrane water electrolysis. *J Power Sources*. 2024;606:234554. https://doi.org/10.1016/j.jpowsour.2024.234554.
20. Paliwal S, Panda D, Bhaskaran S, Vorhauer-Huget N, Tsotsas E, Surasani VK. Lattice Boltzmann method to study the water-oxygen distributions in porous transport layer (PTL) of polymer electrolyte membrane (PEM) electrolyser. *Int J Hydrogen Energy*. 2021;46:22747–22762. https://doi.org/10.1016/j.ijhydene.2021.04.112.
21. Zhang J, Guan X, Yang N. Lattice Boltzmann simulation of oxygen removal from anode porous transport layer in proton exchange membrane electrolyzer. *Chem Eng Sci*. 2024;295:120140. https://doi.org/10.1016/j.ces.2024.120140.
22. Lee JK, Lee Ch, Bazylak A. Pore network modelling to enhance liquid water transport through porous transport layers for polymer electrolyte membrane electrolyzers. *J Power Sources*. 2019;437:226910. https://doi.org/10.1016/j.jpowsour.2019.226910.
23. Stiber S, Balzer H, Wierhake A, et al. Porous transport layers for Proton exchange membrane electrolysis under extreme conditions of current density, temperature, and pressure. *Adv Energy Mater*. 2021;11:2100630. https://doi.org/10.1002/aenm.202100630.
24. Sun Y, Bao C, Jiang Z, Zhang X, Gao T. A two-dimensional numerical study of liquid water breakthrough in gas diffusion layer based on phase field method. *J Power Sources*. 2020;448:227352. https://doi.org/10.1016/j.jpowsour.2019.227352.
25. Wang Z, Wang X, Guo H, et al. A two-dimensional numerical study of oxygen transport in porous transport layer of PEMEC using the phase field method. *Renew Energy*. 2025;247:123044. https://doi.org/10.1016/j.renene.2025.123044.
26. Hoseini Larimi SZ, Ramiar A, Esmaili Q, Shafaghat R. The effect of inlet velocity of water on the two-phase flow regime in the porous transport layer of polymer electrolyte membrane electrolyzer. *Heat Mass Tran*. 2019;55:1863–1870. https://doi.org/10.1007/s00231-018-2436-x.
27. Wu L, Zhang G, Xie B, Tongsh C, Jiao K. Integration of the detailed channel two-phase flow into three-dimensional multi-phase simulation of proton exchange membrane electrolyzer cell. *Int J Green Energy*. 2021;18:541–555. https://doi.org/10.1080/15435075.2020.1854270.
28. Niu Z, Pinfield VJ, Wu B, et al. Towards the digitalisation of porous energy materials: evolution of digital approaches for microstructural design. *Energy Environ Sci*. 2021;14:2549–2576. https://doi.org/10.1039/D1EE00398D.
29. Park J, Kim MJ, Kim Y, Lee S, Park S, Yang W. Insights into bubble dynamics in water splitting. *ACS Energy Lett*. 2025;10:212–237. https://doi.org/10.1021/acsenergylett.4c02736.
30. Frenkel D, Smit B. *Understanding Molecular Simulation: From Algorithms to Applications*. Elsevier; 2023.
31. Kempler PA, Coridan RH, Luo L. Gas evolution in water electrolysis. *Chem Rev*. 2024;124:10964–11007. https://doi.org/10.1021/acs.chemrev.4c00211.

32. Zhan S, Duan H, Pan L, et al. Molecular dynamics simulation of shock-induced microscopic bubble collapse. *Phys Chem Chem Phys*. 2021;23:8446–8455. https://doi.org/10.1039/D1CP00406A.
33. Xiong X, Ma M, Zhang X, Qing S, Wang H, Wang J. Mechanism of charged graphene substrate effects on the stability of interfacial nanobubbles: molecular dynamics simulations. *Langmuir*. 2025;41:8038–8048. https://doi.org/10.1021/acs.langmuir.4c03986.
34. Dixit AK, Das AK. Molecular approach for understanding the stability, collision, and coalescence of bulk nanobubbles. *Langmuir*. 2022;38:16122–16133. https://doi.org/10.1021/acs.langmuir.2c02792.
35. Zhan S, Wang X, Cheng R, Zhou T, Zhang W, Wang J. Investigation of electrolytic hydrogen nanobubbles behavior on heterogeneous wettability surface by using molecular dynamics simulation. *Int J Hydrogen Energy*. 2025;112:160–171. https://doi.org/10.1016/j.ijhydene.2025.02.381.
36. Weijs JH, Snoeijer JH, Lohse D. Formation of surface nanobubbles and the universality of their contact angles: a molecular dynamics approach. *Phys Rev Lett*. 2012;108:104501. https://doi.org/10.1103/PhysRevLett.108.104501.
37. Perez Sirkin YA, Gadea ED, Scherlis DA, Molinero V. Mechanisms of nucleation and stationary states of electrochemically generated nanobubbles. *J Am Chem Soc*. 2019;141:10801–10811. https://doi.org/10.1021/jacs.9b04479.
38. Gadea ED, Perez Sirkin YA, Molinero V, Scherlis DA. Electrochemically generated nanobubbles: invariance of the current with respect to electrode size and potential. *J Phys Chem Lett*. 2020;11:6573–6579. https://doi.org/10.1021/acs.jpclett.0c01404.
39. Li B, Xiang W, Dou X, et al. Coarse-grained molecular dynamics simulation of nucleation and stability of electrochemically generated nanobubbles. *Langmuir*. 2025. https://doi.org/10.1021/acs.langmuir.4c04049.
40. Xu B, Ouyang T, Wang Y, et al. Progresses on two-phase modeling of proton exchange membrane water electrolyzer. *Energy Rev*. 2024;3:100073. https://doi.org/10.1016/j.enrev.2024.100073.
41. Lin R, Huo J, Cai X, Lan S, Hao Z. Numerical study of the effects of wettability and hierarchical porosity on oxygen transport within the porous transport layer of proton exchange membrane electrolyzers. *J Power Sources*. 2024;614:235030. https://doi.org/10.1016/j.jpowsour.2024.235030.
42. Xu C, Wang J, Wang J, Yang K, Gao W, Wang H. Oxygen invasion behavior of anodic porous transport layer in polymer electrolyte membrane water electrolyzer: lattice Boltzmann method simulation. *eTransportation*. 2024:100365. https://doi.org/10.1016/j.etran.2024.100365.
43. Li Q, Bao C, Jiang Z, et al. Numerical study on oxygen transport pattern in porous transport layer of proton exchange membrane electrolysis cells. *eTransportation*. 2023;15:100210. https://doi.org/10.1016/j.etran.2022.100210.
44. Wu Q, Zhang M, Xu X, et al. Effect of channel rib on oxygen removal in 3D porous transport layer of proton exchange membrane electrolysis cell, a numerical investigation. *Int J Hydrogen Energy*. 2025;106:171–185. https://doi.org/10.1016/j.ijhydene.2025.01.450.
45. Li Q, He Y, Zhang L, et al. Optimizing oxygen transport in proton exchange membrane water electrolysis through tailored porosity configurations of porous transport layers. *Appl Energy*. 2024;370:123621. https://doi.org/10.1016/j.apenergy.2024.123621.
46. Yang Y, Ouyang T, Tao D, et al. Improving mass transfer with surface patterning of the porous transport layer for PEM water electrolysis. *Cell Rep Phys Sci*. 2025;6:102433. https://doi.org/10.1016/j.xcrp.2025.102433.
47. Olesen AC, Frensch SH, Kær SK. Towards uniformly distributed heat, mass and charge: a flow field design study for high pressure and high current density operation of PEM electrolysis cells. *Electrochim Acta*. 2019;293:476–495. https://doi.org/10.1016/j.electacta.2018.10.008.
48. Majasan JO, Cho JIS, Dedigama I, Tsaoulidis D, Shearing P, Brett DJL. Two-phase flow behaviour and performance of polymer electrolyte membrane electrolysers: electrochemical and optical characterisation. *Int J Hydrogen Energy*. 2018;43:15659–15672.
49. Lafmejani SS, Olesen AC, Kær SK. VOF modelling of gas–liquid flow in PEM water electrolysis cell micro-channels. *Int J Hydrogen Energy*. 2017;42:16333–16344. https://doi.org/10.1016/j.ijhydene.2017.05.079.
50. Dang DK, Zhou B. Numerical analysis of bubble behavior in proton exchange membrane water electrolyzer flow field with serpentine channel. *Int J Hydrogen Energy*. 2024;88:688–701. https://doi.org/10.1016/j.ijhydene.2024.09.145.
51. Wu L, An L, Jiao D, Xu Y, Zhang G, Jiao K. Enhanced oxygen discharge with structured mesh channel in proton exchange membrane electrolysis cell. *Appl Energy*. 2022;323:119651. https://doi.org/10.1016/j.apenergy.2022.119651.
52. Zhou H, Meng K, Chen W, Chen B. Exploratory research on bubbles migration behavior and mass transfer capacity evaluation of proton exchange membrane water electrolyzer based on a volume of fluid-coupled electrochemical model. *Energy Convers Manag*. 2023;290:117217. https://doi.org/10.1016/j.enconman.2023.117217.
53. Zhou H, Meng K, Chen W, Chen B. Two-phase flow evolution and bubble transport characteristics in flow field of proton exchange membrane water electrolyzer based on volume of fluid-coupled electrochemical method. *J Clean Prod*. 2023;425:138988. https://doi.org/10.1016/j.jclepro.2023.138988.
54. Adamu H, Abba SI, Anyin PB, Sani Y, Yamani ZH, Qamar M. Tuning OER electrocatalysts toward LOM pathway through the lens of multi-descriptor feature selection by artificial intelligence-based approach. *ACS Materials Lett*. 2023;5:299–320. https://doi.org/10.1021/acsmaterialslett.2c00734.
55. Wang T, Wang J, Zhang C, et al. Direct operational data-driven workflow for dynamic voltage prediction of commercial alkaline water electrolyzers based on artificial neural network (ANN). *Fuel*. 2024;376:132624. https://doi.org/10.1016/j.fuel.2024.132624.
56. Krzywanski J, Sosnowski M, Grabowska K, Zylka A, Lasek L, Kijo-Kleczkowska A. Advanced computational methods for modeling, prediction and Optimization—A review. *Materials*. 2024;17:3521. https://doi.org/10.3390/ma17143521.
57. Li Q, Ouyang Y, Lu S, et al. Perspective on theoretical methods and modeling relating to electro-catalysis processes. *Chem Commun*. 2020;56:9937–9949. https://doi.org/10.1039/D0CC02998J.
58. Seyhan M, Akansu YE, Murat M, Korkmaz Y, Akansu SO. Performance prediction of PEM fuel cell with wavy serpentine flow channel by using artificial neural network. *Int J Hydrogen Energy*. 2017;42:25619–25629. https://doi.org/10.1016/j.ijhydene.2017.04.001.
59. Wang B, Xie B, Xuan J, Jiao K. AI-based optimization of PEM fuel cell catalyst layers for maximum power density via data-driven surrogate modeling. *Energy Convers Manag*. 2020;205:112460. https://doi.org/10.1016/j.enconman.2019.112460.
60. Chen J, Lv H, Shen X, Zhang C. Multi-objective optimization design and sensitivity analysis of proton exchange membrane electrolytic cell. *J Clean Prod*. 2024;434:140045. https://doi.org/10.1016/j.jclepro.2023.140045.
61. Wu L, Pan Z, Yuan S, et al. Optimization of dual-layer flow field in a water electrolyzer using a data-driven surrogate model. *Energy and AI*. 2024;18:100411. https://doi.org/10.1016/j.egyai.2024.100411.
62. Zhang G, Wu L, Jiao K, et al. Optimization of porous media flow field for proton exchange membrane fuel cell using a data-driven surrogate model. *Energy Convers Manag*. 2020;226:113513. https://doi.org/10.1016/j.enconman.2020.113513.
63. Cerqueira RFL, Paladino EE. Development of a deep learning-based image processing technique for bubble pattern recognition and shape reconstruction in dense bubbly flows. *Chem Eng Sci*. 2021;230:116163. https://doi.org/10.1016/j.ces.2020.116163.
64. Cui Y, Li C, Zhang W, et al. A deep learning-based image processing method for bubble detection, segmentation, and shape reconstruction in high gas holdup sub-millimeter bubbly flows. *Chem Eng J*. 2022;449:137859. https://doi.org/10.1016/j.cej.2022.137859.

Lizhen Wu received his BS degree (2018) from Dalian Maritime University and his MS degree (2021) from Tianjin University. He is currently pursuing his PhD degree at the Hong Kong Polytechnic University under the supervision of Dr. Liang An. His current research focuses on water electrolyzers.

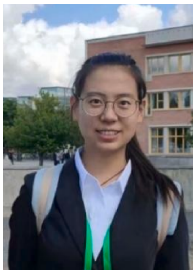

Qing Wang received her BS degree (2018) from Tianjin University and her MS degree (2021) from Tsinghua University. She is currently pursuing her PhD degree at the Hong Kong Polytechnic University under the supervision of Dr. Liang An. Her current research focuses on water electrolyzers.

Wenzhi Li received his BS degree (2019) and MS degree (2022) from the North China Electric Power University, Beijing. He is currently pursuing his PhD degree at the Hong Kong Polytechnic University under the supervision of Dr. Liang An. His current research focuses on ammonia fuel cells.

Mingcong Tang received his BS degree (2020) from the University of California, San Diego, and his MS degree (2022) from the University of Michigan, Ann Arbor. He is currently pursuing his PhD degree at the Hong Kong Polytechnic University under the supervision of Dr. Liang An. His current research focuses on aqueous Zinc metal-based batteries.

Liang An received his BS degree (2008) from Harbin Institute of Technology and his PhD degree (2012) from The Hong Kong University of Science and Technology. He is currently an Associate Professor in the Department of Mechanical Engineering at The Hong Kong Polytechnic University. His research interests include advanced energy conversion and storage technologies, such as fuel cells and batteries.